Analysis of In-situ Electric Field and Specific Absorption Rate in Human Models for Wireless Power Transfer System with Induction Coupling

Tetsu Sunohara[1], Akimasa Hirata[1], Ilkka Laakso[1], and Teruo Onishi[2]

1: Nagoya Institute of Technology, Department of Computer Science and Engineering, Nagoya, Aichi 466-8555, Japan

2: Research Laboratories, NTT DOCOMO, INC., 3-6 Hikari-no-Oka, Yokosuka, Kanagawa 239-8536, Japan

Corresponding Author: Akimasa Hirata

Address: Nagoya Institute of Technology, Gokiso-cho, Showa-ku, Nagoya, Aichi 466-8555, Japan

Tel & Fax: +81-52-735-7916

E-mail: ahirata@nitech.ac.jp

Abstract

The present study investigates the specific absorption rate (SAR) and the in-situ electric field in anatomically based human models for the magnetic field from an inductive wireless power transfer system developed on the basis of the specifications of the Wireless Power Consortium. The transfer system consists of two induction coils covered by magnetic sheets. Both the waiting and charging conditions are considered. The transfer frequency considered in this study is 140 kHz, which is within the range where the magneto-quasi-static approximation is valid. The SAR and in-situ electric field in the chest and arm of the models are calculated by numerically solving the scalar potential finite difference equation. The electromagnetic modelling of the coils in the wireless power transfer system is verified by comparing the computed and measured magnetic field distributions. The results indicate that the peak value of the SAR averaged over a 10 g of tissue and that of the in-situ electric field are 72 nW/kg and 91 mV/m for a transmitted power of 1 W, respectively, corresponding to the allowable transmitted power of 28 MW and 43 kW. The computational results show that the in-situ electric field in the chest is the most restrictive factor when compliance with the wireless power transfer system is evaluated according to international guidelines.

1   INTRODUCTION

Recent technological advancements have enabled effective wireless transfer of power via radio waves, which has many potential everyday applications (Shinohara 2011). Attention is required regarding the safety of human against radio waves used in the wireless power transfer (Laakso *et al.* 2012, Christ *et al.* 2013, Park *et al.* 2013) because the expected transmitted power is much greater than that actually used, for instance, in wireless communications. In particular, the maximum allowable transmitted power that satisfies human exposure limits prescribed in the international safety guidelines/standards (ICNIRP 1998, 2010, IEEE 2005) is important in the design of wireless power transfer systems. The frequency band considered for wireless power transfer with magnetic induction is in the range of 100 kHz and higher. One of the possible applications is the charging of mobile phones, which has already been implemented in consumer products in Japan and other countries (Okudake-Juden 2013, Qi Wireless Charging 2013). Users can charge their mobile phones not only in their homes but also in public areas and shops. Currently, the typical value of maximum transmitted power in Japan is 5 W, which is projected to be increased to 50 W or higher, to apply the system to tablets, laptop PCs, and similar devices. The external field strength from such systems may exceed the reference level or the maximum permissible exposure limit specified in the international guidelines/standards (ICNIRP 1998, 2010, IEEE 2005). In this case, compliance with the basic restrictions, that is, the limits for both

the specific absorption rate (SAR) averaged over a 10 g of tissue and the in-situ (internal) electric field should be evaluated (ICNIRP 1998, 2010, IEEE 2002, 2005). Both the SAR and in-situ electric field are used as a metric for human protection at frequencies from 100 kHz to 10 MHz.

Previous studies that evaluated human exposure to electromagnetic fields emitted from wireless power transfer have concentrated on resonant-type (Kurs *et al.* 2007) wireless power transfer systems (Laakso *et al.* 2012, Christ *et al.* 2013, Park *et al.* 2013). Previous studies did not consider realistic wireless power transfer systems in their evaluation. In addition, the resonant-type systems feature larger coils and longer distances compared with the inductive power transfer systems already being used in consumer products. The inductive systems produce much more localised magnetic fields, which locally induce an electric field and SAR in the body when the induction coils are placed near it. This condition prompts particular emphasis on the evaluation of partial-body exposure, rather than the whole-body exposure considered in larger resonant-type systems. Currently, no study has investigated human exposure to magnetic fields from inductive power transfer systems. In our previous study, preliminary results were presented for the SAR in a homogeneous cube, which simulated a human trunk (Hirata *et al.* 2013b).

In the current study, the magnetic field distribution generated from an inductive wireless power transfer system, which is developed on the basis of the Wireless Power Consortium (WPC) specifications (Qi Wireless Charging 2013), is first simulated and validated by comparison with the measurements. A two-step magneto-quasi-static computational method comprising the method of moments (MoM) and the scalar potential finite difference (SPFD) method (Laakso *et al.* 2012) is then used to investigate the in-situ electric field and SAR in anatomically based human models.

2 METHOD AND MODEL

2.1 Modelling of coils

Figure 1(a) shows the geometry of the two coils in a wireless power transfer system with induction coupling. The coils are modelled using FEKO (EMSS-SA, Stellenbosch, South Africa) as perfectly conducting wires with a radius of 0.3 mm, and the system is excited by a voltage source located at port 1. The inner and outer radii of the coils are $R_i = 6$ mm and $R_o = 20$ mm, and the number of turns is 20. The separation between the two coils D_z is 3.5 mm. Furthermore, the coils are covered by square-shaped magnetic sheets, as shown in figure 1(b). The magnetic sheet dimensions are 55 mm × 55 mm × 0.6 mm, and their relative permeability is 7000. The distance between the coil and the magnetic sheet is 0.5 mm. The power to be transmitted is normalised to 1 W. We note that the magnetic field and the in-situ electric field

are proportional to the square root of the transmitted power, and the induced SAR is directly proportional to the transmitted power. In addition to the 'charging' condition, the 'waiting' condition is simulated by removing the coil and the magnetic sheet at the receiving side.

A resistance of 1 Ω with a capacitance of 44.6 nF is installed at port 1 and port 2 of the receiving coil. In the measurement, these ports are connected to their respective active circuit to maintain effective power transfer as much as possible. However, these circuits are not modelled in this study. The impedance of the coil without the circuit is the lowest, corresponding to the highest coil current for a fixed transmitted power. This assumption results in the largest magnetic field amplitude emitted from the system or the worst case exposure because the in-situ electric field and SAR in the wireless power transfer system is mainly characterised by the magnetic field (Hirata *et al.* 2013a).

2.2   Computational methods

The magneto-quasi-static approximation is applicable in the 100-kHz frequency band, that is, the displacement current is negligible when compared with the conduction current (Hirata *et al.* 2013a). The magnetic field generated by the induction coils is first obtained using the MoM/finite-element method without considering the human model. The in-situ electric field is then computed by numerically solving the SPFD equation system using the multi-grid method (Laakso and Hirata 2012a). The simplification of using the external magnetic field without the human body is based on the fact that the human body behaves as a poor conductor, and thus, the external magnetic field is not disturbed by the body. In addition, the in-situ electric field and SAR are primarily induced by the external magnetic field rather than the external electric field (Hirata *et al.* 2013a). We note that this simplification is valid even in the 10-MHz band for wireless power transfer with magnetic resonance (Laakso *et al.* 2012). When compared with the full-wave analysis (e.g., the finite-difference time-domain method), the source magnetic field has to be solved only once for a single-system configuration, which leads to a greatly reduced computational effort, particularly in the study of a variety of human-body models/human–coil positions. Computing each exposure scenario would takes 45 s. We note that the number of multigrid levels is four, and the iteration continues until the relative residual is less than 10^{-6}. The estimated error in the electric field for this relative residual is less than 0.5% (Laakso and Hirata 2012a). The effect of the 2-mm model resolution may cause a computational uncertainty of less than a few dozen percent when the maximal in-situ electric field is estimated, as presented by Laakso and Hirata (2012c). We note that this computational uncertainty includes the uncertainty caused by the anatomical modelling as well as that obtained by computation.

2.3   Anatomically based human-body models

Whole-body voxel models based on magnetic resonance images for different genders and races are considered. The present study uses the Japanese male model TARO (Nagaoka *et al.* 2004) and the European male and female models DUKE and ELLA, respectively, (Christ *et al.* 2010). The height and weight of the TARO model are 1.73 m and 65 kg, respectively. The heights and weights of the DUKE and ELLA models are 1.74 m and 70 kg and 1.60 m and 58 kg, respectively. These models have a resolution of 2 mm and consist of 51–70 anatomical tissues/organs. The tissue conductivities are obtained from the study of Gabriel (1996). Schmid *et al.* (2013) suggested that the Gabriel model can underestimate the skin conductivity by a large margin. In the present study, the conductivity of the skin was set to represent that of a wet skin, which is slightly higher than the conductivity of subcutaneous fat at the studied frequency.

2.4   Exposure conditions and dose metrics

Occasional exposure to the magnetic fields in the power transfer system is assumed to occur in the chest and arm regions. Under this assumption, the SAR and in-situ electric field in these regions must be compared to determine the region where the SAR and the electric field are the highest.

Figures 2(a) and (b) show the exposure conditions on the chest of a human model. Figure 2(a) shows that the transmitting coil is located in front of the chest at positions labelled A to I. The separation between the positions is 60 mm, and the distance between the coil and the chest is 10 mm. Figure 2(b) shows that the coil is placed in position E, and the distance between the chest and the coil is varied from 10 to 140 mm. Figure 3 shows the exposure condition of the arm. Two positions of the transmitting coil in proximity to the hand and forearm are considered. The coil is located below the palmar side of the hand or forearm at a distance of 10 mm.

In RF continuous-wave exposure, the SAR is the compliance-determining metric for frequencies above 100 kHz. To assess the compliance of the maximum localised SAR (6-min average), the ICNIRP basic restriction (1998) applies to 10 g of 'contiguous' tissues, whereas the IEEE basic restriction (2005) applies to a 10-g volume 'in the shape of a cube'. In the present study, the algorithm prescribed in the IEEE standard is used to calculate the mass-averaged SAR over a volume with a cubic shape because no clear description is given in the ICNIRP guidelines (1998). For frequencies below 10 MHz, ICNIRP (2010) recommends the determination of the in-situ electric field as a vector average of the electric field in a small contiguous tissue volume of $2 \times 2 \times 2$ mm^3 (instantaneous value). Even though the ICNIRP recommends the use of the '99th percentile' value of the in-situ electric field to eliminate numerical staircasing error, we use the maximum electric field because the '99th percentile' value may underestimate the in-situ electric field for localised exposure. Instead, the smoothing algorithm is applied to the conductivity of the tissue to suppress the staircasing error as much as

possible (Laakso and Hirata 2012b).

SAR evaluation may not be necessary under the waiting condition because the SAR should be averaged over 6 min. The electromagnetic field emitted under the waiting condition is a pulse signal that searches if a receiver exists. Thus, the actual time-averaged value of the SAR is lower than that presented in the following sections, where continuous wave is assumed. However, both metrics are evaluated in this study because the duty cycle and amplitude in the waiting condition is not currently well standardised.

2.5   Experimental procedure for validation

We use the transmitting and receiving coils that conform to the WPC (2013) specifications for measurements. The magnetic probe 11941A (Agilent technology, USA), whose frequency range is from 9 kHz to 30 MHz and the antenna factor deviation is ±2 dB, is used to measure the magnetic field distribution around the coils. First, the frequency components of the charging and waiting conditions are measured to confirm the fundamental frequency when a transferred power of 1 W is considered. Then, the magnetic field distributions at the fundamental frequency are measured at intervals of 10 mm on the *xy* and *yz* planes. We note that the repeatability of the scanner is ±0.01 mm.

3   COMPUTATIONAL RESULTS

3.1   Confirmation of the electromagnetic modelling

To confirm the magnetic field distribution generated by the transfer system, the measured and computed results under both the charging and waiting conditions are compared. The computed and measured magnetic fields are normalised by the maximum amplitude. Direct comparison of the magnetic field amplitudes is not possible because the magnetic field is characterised by the coil current, which cannot be measured, and is affected by the impedance of the internal active circuit. This circuit is not modelled in the computational electromagnetic simulation. We note that the computed amplitude of the magnetic field is larger than that of the measurement by a factor of two or more (depending on the impedance of the internal circuit). The 140-kHz frequency is chosen in the comparison. The computed results are averaged over an area of 5 mm × 36 mm to coincide with that of the probe (Agilent11941A).

The computed and measured magnetic field distributions under the waiting and charging conditions are shown in figures 4 and 5, respectively. These figures show the good agreement between the measured and computed results under the waiting condition and the fair agreement under the charging condition. One of the possible reasons for this difference is attributed to some factors such as the case surrounding the coils and the circuit board in the measurement, which are not considered in the electromagnetic modelling.

We should note that the magnetic field distribution without the magnetic sheet is symmetrical. Thus, the disturbance in the field is primarily attributed to the insertion of the magnetic sheet. In addition, the magnetic field intensity becomes quite stronger around the feed points of the coils. By comparing the charging and waiting condition results shown in figures 4 and 5, we can observe that the magnitude of the magnetic field under the charging condition is smaller than that under the waiting condition because most of the transmitted power is received at the receiving coil. From the computational results, for example, in the waiting condition for a transmitted power of 5 W, which is a typical value for maximum power transfer in Japan, the human model is exposed to a magnetic field with a local maximum strength of approximately 44.7 A/m. This amplitude exceeds the reference level of 21 A/m (instantaneous value) and 5 A/m (6-min average) defined in the ICNIRP guidelines (1998, 2010) for the general public; thus, computational assessment of the SAR and in-situ electric field in relation to the basic restrictions is essential.

3.2   SAR and in-situ electric field in different body regions

Table I lists the computation results of the SAR and in-situ electric field in front of the chest of the TARO model in various positions. The results show that both the SAR and in-situ electric field are larger under the waiting condition than those under the charging condition. We should note that the presented SAR values are calculated for the case when the transmitter is continuously transmitting 1 W. In reality, the field waveform in the waiting condition would have a pulse shape, and hence, the SAR averaged over a 6-min period would be smaller than that presented in the table, depending on the duty cycle. The maximum values of the 10-g averaged SAR and in-situ electric field are 49.9 nW/kg and 80.7 mV/m, respectively, at position H, which is at the lower centre of the chest. The average values of the SAR and in-situ electric field under the waiting condition are 29.2 nW/kg and 47.5 mV/m, respectively.

The SAR distribution in the chest when the coil is at position E is shown in figures 6(a) and (b) under the charging and waiting conditions, respectively. By comparing these figures, we can observe that the SAR distributions are concentrated at the centre of the chest, which is the region closest to the coil. Furthermore, the SAR values under the waiting condition are higher, as expected. Similarly, figures 6(c) and (d) show the in-situ electric field distribution in the chest under the charging and waiting conditions, respectively. These figures show that the in-situ electric field distributions are similar to the SAR distributions. We note that the whole-body averaged SAR, which is a metric for the whole-body exposure, is 2.89 pW/kg at the maximum. When the ratio to the basic restriction is considered, the local SAR averaged over a 10 g of tissue is found to be restrictive by a factor of 18.

Figures 7 and 8 show the distributions of the SAR and in-situ electric field in the forearm

and hand of the TARO model under the waiting condition, respectively. The distributions under the charging condition are not presented because the induced values are smaller, as shown in figure 6. Figures 7 and 8 show that the induced values are greater in the region closest to the transmitting coil. Table 2 lists the SAR and in-situ electric field for the hand, forearm, and chest of the TARO model. Both the SAR and in-situ electric field are larger under the waiting condition than those under the charging condition.

3.3 Variability among the human models

The computational results for various positions on the chest of the DUKE and ELLA models under the waiting condition are listed in Table 3. The computation results under the charging condition are not listed because the SAR and in-situ electric field are smaller than those under the waiting condition, similar to those observed in the TARO model. For the DUKE model, the maximum values of the 10-g averaged SAR is 71.8 nW/kg for position B and the in-situ electric field is 91.2 mV/m for position H, respectively. On the other hand, for the ELLA model, the maximum values of the 10-g averaged SAR and in-situ electric field are 46.3 nW/kg and 80.0 mV/m, respectively, both obtained at position B. The average values of the in-situ electric field in the DUKE and ELLA models are 64.5 mV/m and 56.8 mV/m, respectively. The computational results of the arms of the DUKE and ELLA models are omitted as not much difference is observed compared with those of the SAR and in-situ electric field of the TARO model.

To discuss the variability of the in-situ electric field in terms of tissue conductivity, we performed a sensitivity analysis of the tissue conductivity on the in-situ electric field. We considered position H in the TARO model with eight different conductivity combinations. The skin conductivity was set to be either wet or dry. The fat was considered to be either infiltrated or not infiltrated with blood. The bone conductivity was considered to be either cortical or cancellous bone. We note that the reference value in our computations corresponded to dry skin and infiltrated fat, and both cortical and cancellous bone were present in the model. For these eight cases in the TARO model, the in-situ electric field was varied from -0.06% to +30.9% for position H.

3.4 Dependence of the SAR and in-situ electric field on distance

Figure 9 shows the dependence of the peak 10-g averaged SAR on the distance between the body and the transmitting coil when the system is located at position E in front of the chest. The peak averaged SAR under the waiting condition is higher than that under the charging condition, similar to the distribution shown in figure 6. The peak SARs under the charging and waiting conditions at $D = 10$ mm are 1.1 and 41.5 nW/kg, respectively, and decrease exponentially with

distance under both conditions.

Figure 10 shows that the maximum magnitudes of the in-situ electric field are 9.9 and 57.8 mV/m under the charging and waiting conditions, respectively, at $D = 10$ mm. Similar to the SAR characteristics shown in figure 9, the in-situ electric field under the waiting condition is higher than that under the charging condition. We note that the maximum electric field is induced in the subcutaneous fat in all exposure scenarios.

4   DISCUSSION

Table 1 indicates that the maximum values of the in-situ electric field are obtained in position H in front of the chest [figure 2(a)]. In this position, the maximum in-situ electric field appears in the fat and bone because these tissues have lower conductivity compared with the muscle tissue. The same tendency can be observed in positions B and E. Table 2 indicates that both the SAR and the in-situ electric field in the chest are larger than those in the hand and forearm, which is attributed to the area through which the magnetic flux passes the human body (Laakso *et al.* 2012). Therefore, evaluation of the in-situ electric field and SAR in the chest is essential. In addition to the TARO model, the maximum values of the in-situ electric field and SAR in the DUKE and ELLA models are obtained for positions in the centre of the chest. From these results, we can assume that the coil position in which the maximum induced value occurs is always located at the centre of the chest.

In all cases considered in this study, the peak 10-g averaged SAR for a 1-W power transfer is at most 71.8 nW/kg, which is a very low value compared with the basic restriction of 2 W/kg (ICNIRP 1998) and corresponds to the allowable transmitted power of 28 MW. On the other hand, the ratio of the in-situ electric field, which is at a maximum of 91.2 mV/m, to the basic restriction of 18.9 V/m (ICNIRP 2010) is 4.8×10^{-3}, corresponding to the allowable transmitted power of 43 kW. These results indicate that the in-situ electric field is a more relevant exposure metric than the peak 10-g averaged SAR. We note that this value decreases exponentially with the increase in the coil–body distance and increases proportionally to the square root of the transferred power.

The computed in-situ electric field is affected by several uncertainty factors. We have previously shown that for a computational technique similar to that employed in this study, the uncertainty due to the resolution of the computational grid is much smaller than that caused by the model anatomy or tissue conductivity (Laakso and Hirata 2012c). To investigate the uncertainties caused by these factors, we performed a sensitivity analysis that suggested that the variability caused by the model anatomy was 13% (three anatomical models), and the variability caused by the tissue conductivity was 30% (eight conductivity combinations). Although these variations were derived from limited number of cases, they are still indicative of the magnitude

of the computational uncertainty. Hence, our conclusion that the in-situ electric field is much smaller than the basic restriction is unaffected by the potential uncertainty in the computed values.

In conclusion, this study has investigated the SAR and in-situ electric field in anatomically based human-body models of the magnetic field emitted from wireless power transfer system with induction coupling. The coils were modelled based on the WPC specifications (Qi Wireless Charging 2013). By comparing the measured and computed magnetic field distributions, the effectiveness of the computational modelling was confirmed. The computational results obtained herein suggest that both the SAR and the in-situ electric field are much smaller than the basic restrictions even though the local maximum magnetic field that the human body is exposed to exceeds the reference level prescribed by international guidelines. In addition, the results confirm that evaluation of the in-situ electric field in the chest is essential to monitor compliance with the basic restrictions.

REFERENCE

Christ A Kainz W, Hahn E G, Honegger K, Zefferer M, Neufeld E, Rascher W, Janka R, Bautz W, Chen J, Keifer B, Schmit P, Hollenbach H P, Shen J, Oberle M, Szczerba D, Kam A, Guag J W and Kuster N 2010 The Virtual Family - development of surface - based on anatomical methods of two adults and two children for dosimetric simulations *Phys. Med. Biol.* **55** 22-38

Christ A, Douglas M, Nadakuduti J and Kuster N 2013b Assessing Human Exposure to Electromagnetic Fields From Wireless Power Transmission Systems Proc. IEEE **101** 1482-93

Hirata A, Ito F and Laakso I 2013a Confirmation of quasi-static approximation in SAR evaluation for a wireless power transfer system *Phys. Med. Biol.* **58** 241-9

Hirata A, Sunohara T, Laakso I and Onishi T 2013b SAR in a simplified human model due to wireless power transfer with induction coupling *Proc. Europ. Conf. Antennas and Propagation,* 1769-72

A. Hirata, J. Hattori, I. Laakso, A. Takagi, and T. Shimada 2013c Computation of induced electric field in the sacral nerve activation, Phys. Med. Biol., **58** 7745-55

ICNIRP 1998 Guidelines for limiting exposure to time-varying electric, magnetic and electromagnetic fields (up to 300 GHz) *Health Phys.* **74** 494-522

ICNIRP 2010 Guidelines for limiting exposure to time-varying electric and magnetic field (1 Hz

to 100 kHz) *Health Phys.* **99** 818-36

IEEE 2002 IEEE Standard for safety Levels with Respect to Human Exposure to Electromagnetic Fields, 0-3 kHz IEEE Standards C95.6

IEEE 2005 IEEE Standard for safety Levels with Respect to Human Exposure to Radio Frequency Electromagnetic fields, 3 kHz to 300 GHz IEEE Standards C95.1

Kurs A, Karalis A, Moffatt R, Joannopoulos J D, Fisher P and Soljačić M 2007 Wireless Power Transfer via Strongly Coupled Magnetic Resonances *Science* **317** 83-6

Laakso I and Hirata A 2012a Fast multigrid-based computation of the induced electric field for transcranial magnetic simulation *Phys. Med. Biol.* **57** 7753-65

Laakso I and Hirata A 2012b Reducing the staircasing error in computational dosimetry of low-frequency electromagnetic fields *Phys. Med. Biol.* **57** N25-34

Laakso I and Hirata A 2012c Computational analysis of thresholds for magnetophosphenes *Phys. Med. Biol.* **57** 6147-65

Laakso I, Tsuchida S, Hirata A and Kamimura Y 2012 Evaluation of SAR in a human body model due to wireless power transmission in the 10 MHz band *Phys. Med. Biol.* **57** 4991-5002

Nagaoka T, Watanabe S, Sakurai K, Kunieda E, Watanabe S, Taki M and Yamanaka Y 2004 Development of realistic high-resolution whole-body voxel models of Japanese adult males and females of average height and weight , and application of models to radio-frequency electromagnetic-field dosimetry *Phys. Med. Biol.* **49** 1-15

Okudake-Juden 2013 NTT DOCOMO http://www.nttdocomo.co.jp/english/service/convenience/wireless_charge/index.html/

Park S W, Wake K and Watanabe S 2013 Incident Electric Field Effect and Numerical Dosimetry for a Wireless Power Transfer System Using Magnetically Coupled Resonances *IEEE Trans. Microw. Theory Tech.* **61** 3461-9

Schmid G, Cecil S and Überbacher R 2013 The role of skin conductivity in a low frequency exposure assessment for peripheral nerve tissue according to the ICNIRP 2010 guidelines *Physics in Medicine and Biology* **58** 4703

WPC specifications, 2013 System description wireless power transfer volume 1 version 1.1.2.

Shinohara N 2011 Power without wires *IEEE Microw. Mag.* **12** S64-73

Wireless Power Consortium 2013 http://www.wirelesspowerconsortium.com/

Figure and Table Captions

Fig. 1. (a) Configuration of the transmitting and receiving coils and (b) geometry of the magnetic sheet.

Fig. 2. Computational conditions for the chest in (a) various positions and (b) distance variations of the coil.

Fig. 3. Computational condition for the arm.

Fig. 4. Computed magnetic field distribution on the (a) xy plane and (b) yz plane under the charging condition and on the (c) xy plane and (d) yz plane under the waiting condition.

Fig. 5. Measured magnetic field distribution on the (a) xy plane and (b) yz plane under the charging condition and on the (c) xy plane and (d) yz plane under the waiting condition.

Fig. 6. SAR distributions under the (a) charging and (b) waiting conditions. Electric field distributions under the (c) charging and (d) waiting conditions in the chest of the TARO model.

Fig. 7. (a) SAR and (b) in-situ electric field distributions in the hand of the TARO model under the waiting condition.

Fig. 8. (a) SAR and (b) in-situ electric field distributions in the forearm of the TARO model under the waiting condition.
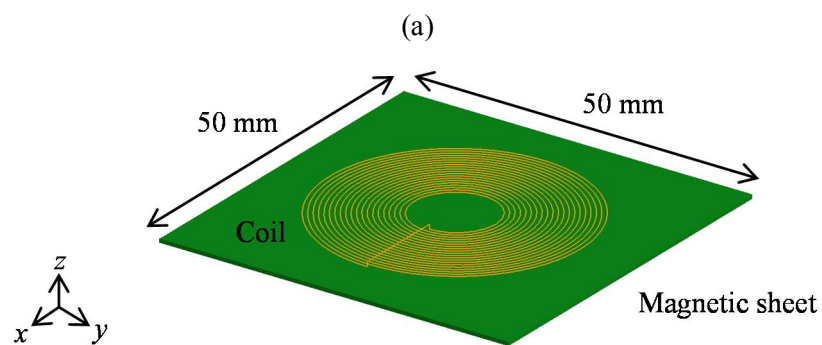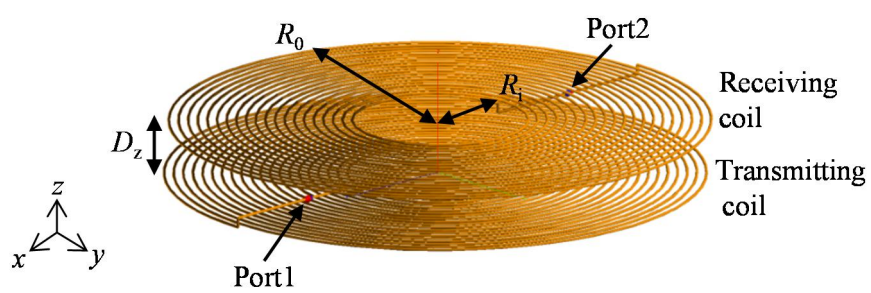
Fig. 9. Dependence of the peak 10-g averaged SAR on the coil–body separation.

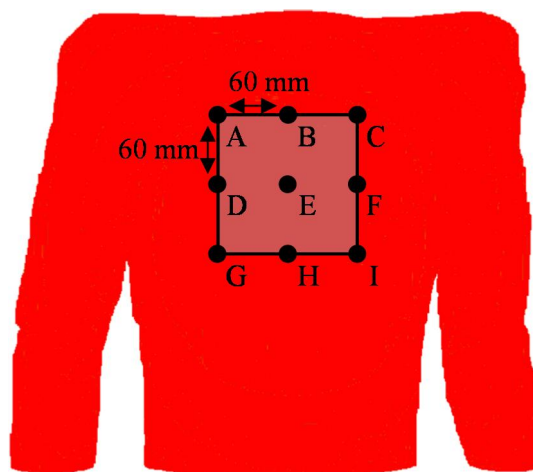Fig. 10. Dependence of the peak in-situ electric field on the coil–body separation.

Table 1. Peak 10-g averaged SAR and maximum in-situ electric field for various positions of the chest in the TARO model.

Table 2. Peak 10-g averaged SAR and maximum in-situ electric field for the various body regions in the TARO model.
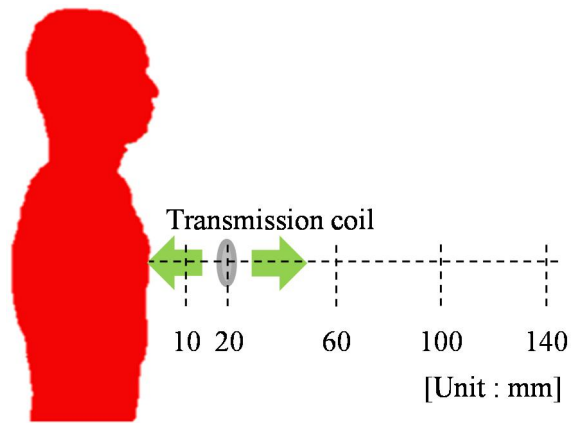
Table 3. Peak 10-g averaged SAR and maximum in-situ electric field for various positions of (a) the DUKE and (b) ELLA models under the waiting condition.
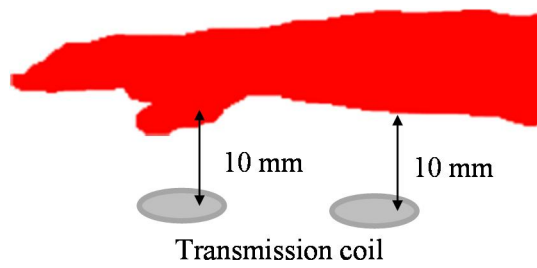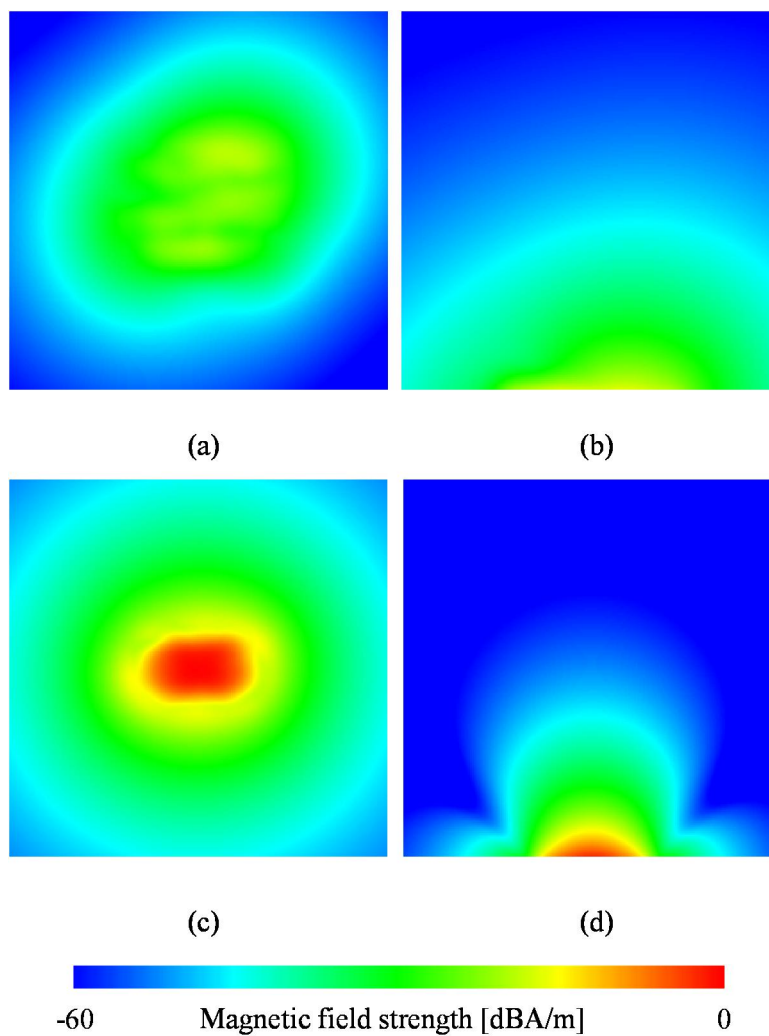
R_0 Port2   Receiving coil

R_i

D_z

Transmitting coil

z

x y

Port1

(a)

50 mm   50 mm

z

x y

Coil   Magnetic sheet

(b)

Figure 1

60 mm

60 mm

A B C

D E F

G H I

(a)

Transmission coil

10 20 60 100 140

[Unit : mm]

(b)

Figure 2

10 mm 10 mm

Transmission coil

Figure 3

(a)

(b)

(c)

(d)

-60   Magnetic field strength [dBA/m]   0

Figure 4

(a)

(b)

(c)

(d)

-60　　Magnetic field strength [dBA/m]　　0

Figure 5

(a)   (b)

4.0×10^{-9} SAR [W/kg] 4.0×10^{-11}

(c)   (d)

0   Electric field [V/m]   0.025

Figure 6

SAR [W/kg]

5.0×10^{-8}

5.0×10^{-10}

Electric field [V/m]

0.025

0

(a)

(b)

Figure 7

SAR [W/kg]

5.0×10^{-8}

5.0×10^{-10}
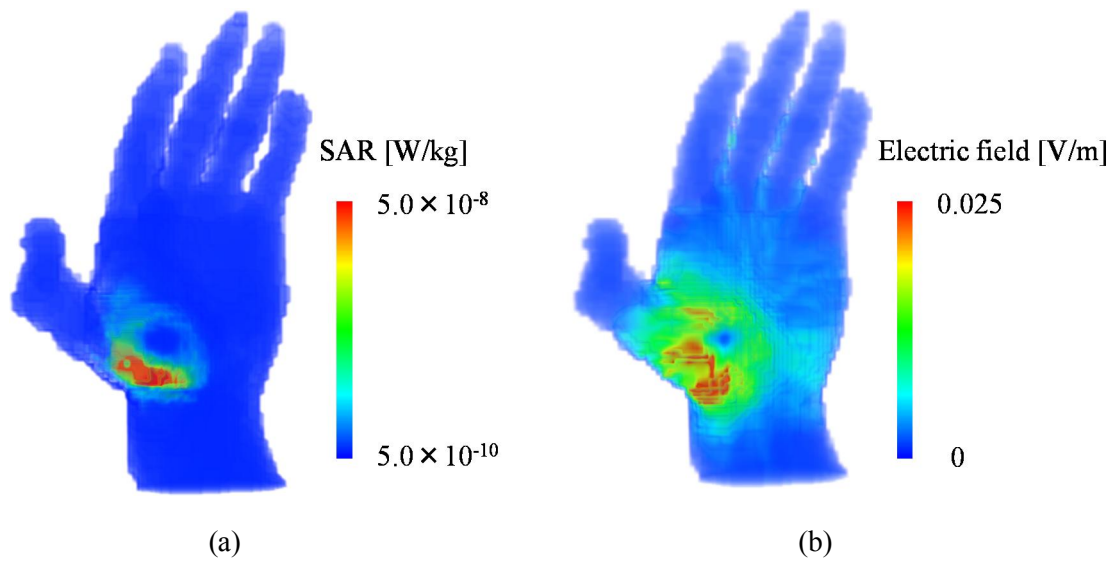
Electric field [V/m]

0.025

0

(a)

(b)
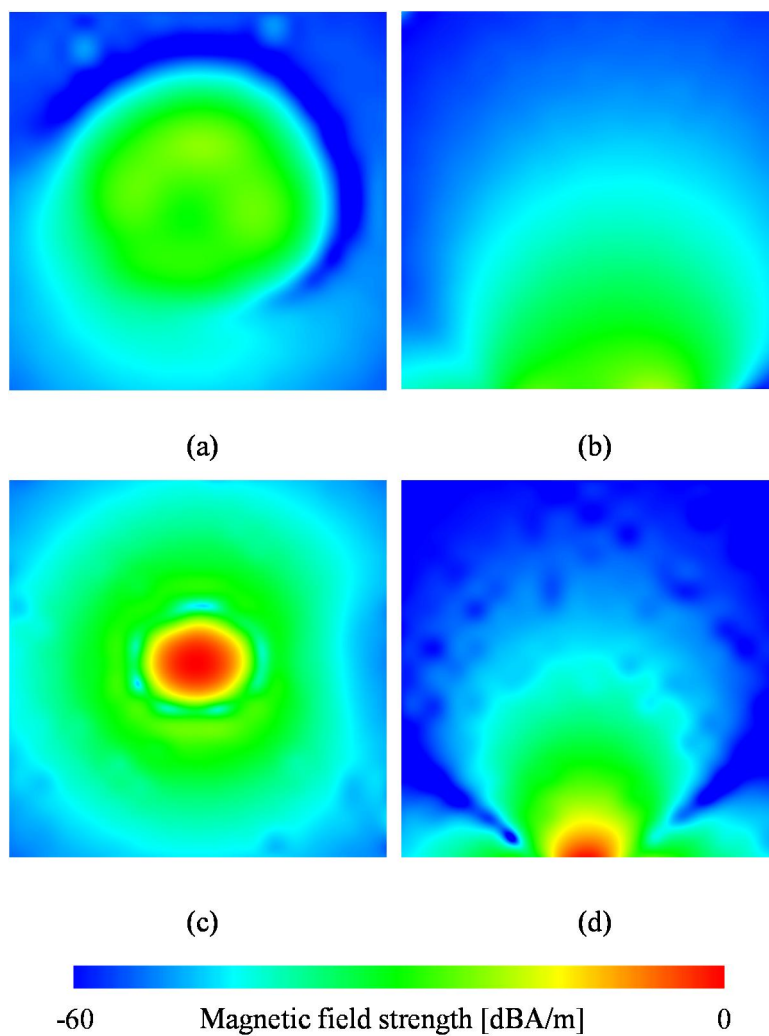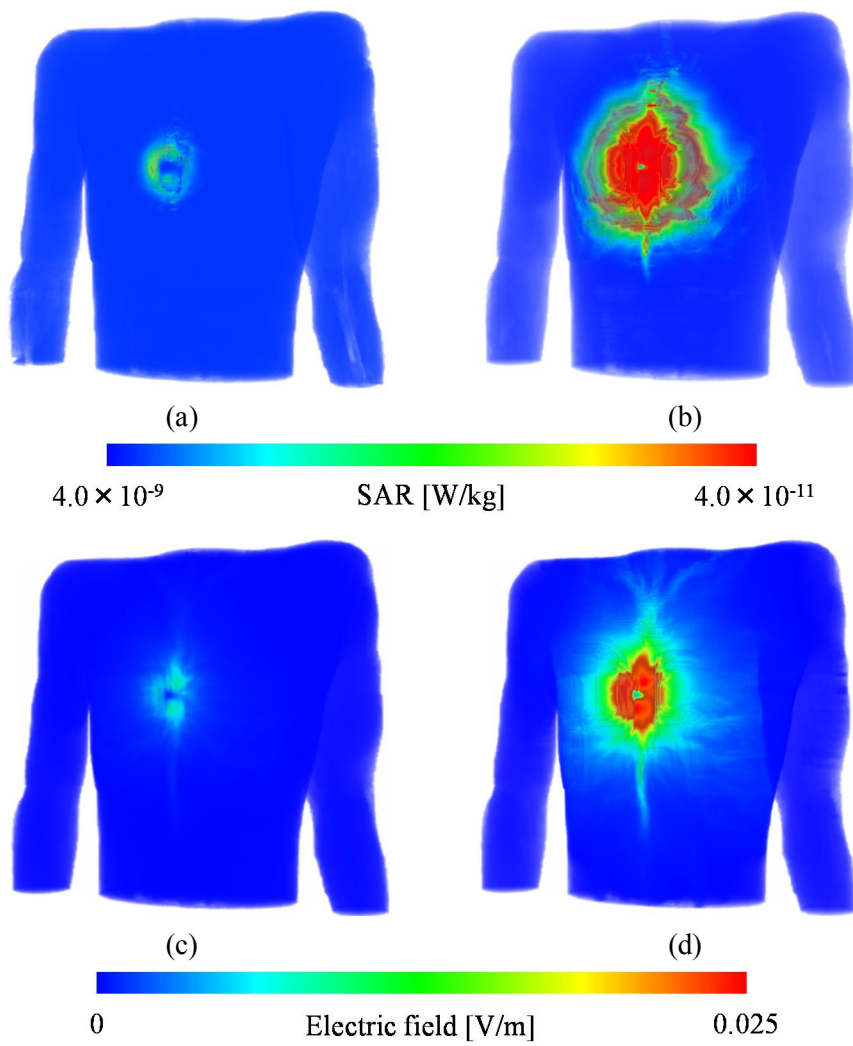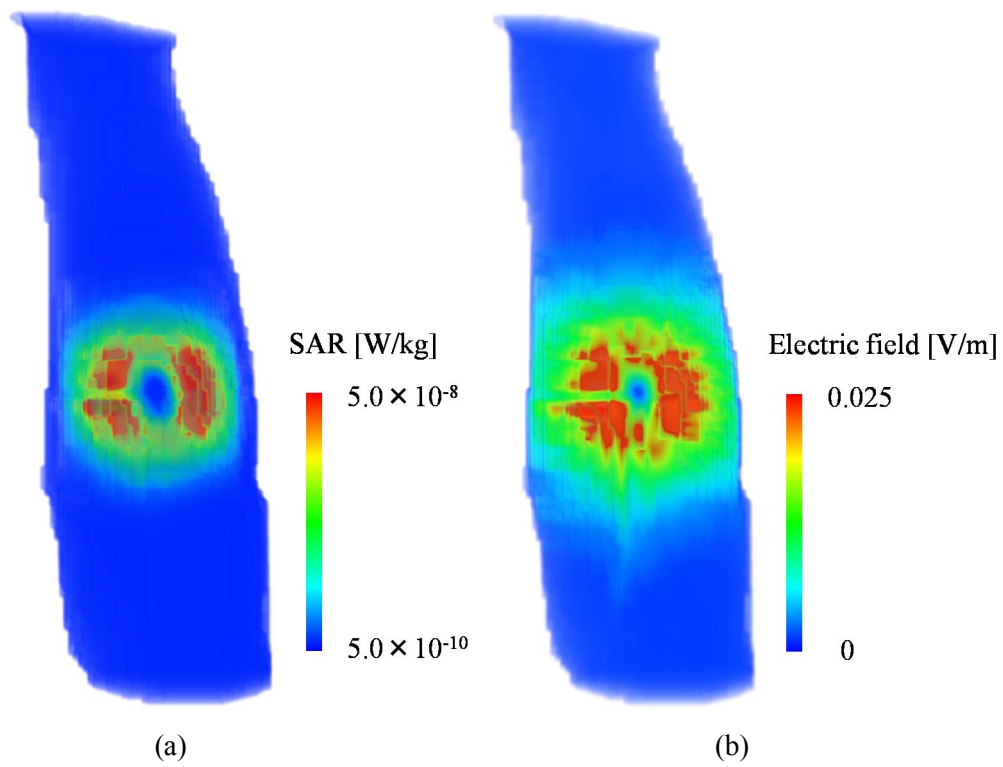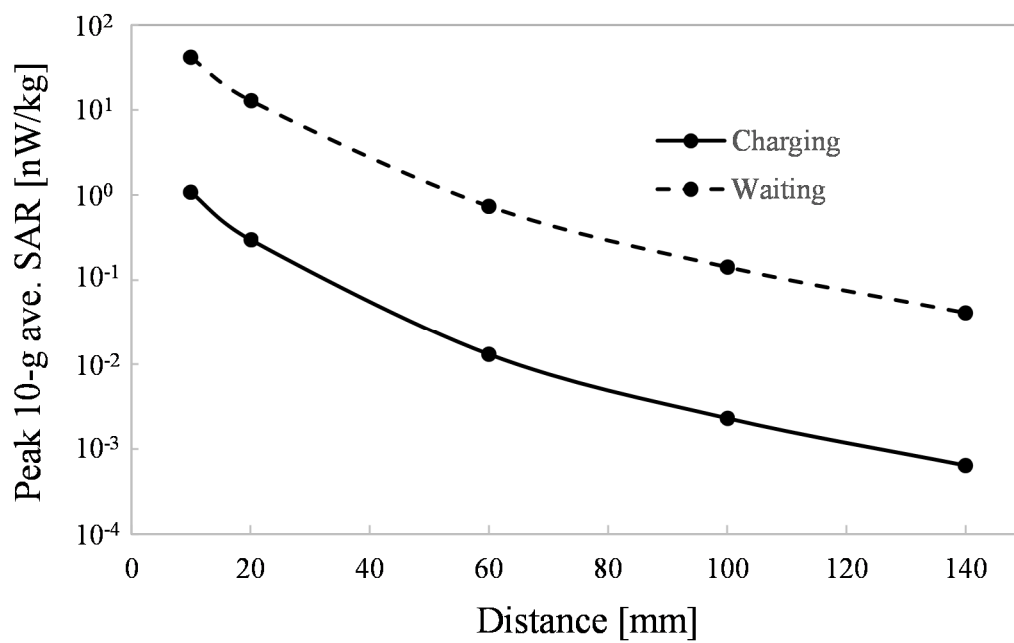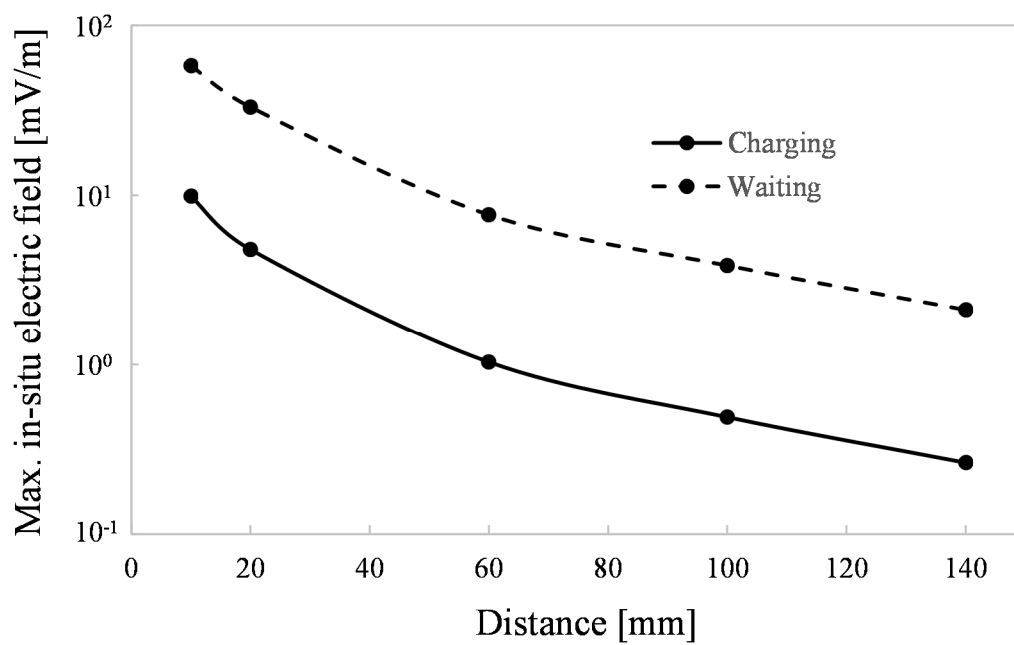
Figure 8

Figure 9

Figure 10

Table 1

	Peak 10-g average SAR [nW/kg]		Maximum in-situ electric field [mV/m]	
	Charging	Waiting	Charging	Waiting
A	0.49	18.5	9.1	44.3
B	0.47	18.4	7.2	45.4
C	0.77	29.7	7.1	41.2
D	0.51	19.8	6.8	39.1
E	1.1	41.5	9.9	57.8
F	0.72	27.7	6.9	37.9
G	0.66	26.9	6.7	38.2
H	1.3	49.9	12.2	80.7
I	0.79	31.1	7.6	42.7

Table 2

TARO	Peak 10-g average SAR [nW/kg]		Maximum in-situ electric field [mV/m]	
	Charging	Waiting	Charging	Waiting
Chest (E position)	1.1	41.5	9.9	57.8
Forearm	0.62	24.9	5.8	35.2
Hand	0.35	13.7	4.5	29.2

Table 3

(a)

	Peak 10-g average SAR [nW/kg]	Maximum in-situ electric field [mV/m]
A	24.0	50.9
B	71.8	87.1
C	28.7	54.4
D	46.5	50.4
E	63.6	86.8
F	48.1	58.1
G	36.5	51.5
H	67.0	91.2
I	38.2	50.1

(b)

	Peak 10-g average SAR [nW/kg]	Maximum in-situ electric field [mV/m]
A	13.3	42.1
B	46.3	80.0
C	14.2	48.1
D	9.6	36.6
E	40.8	66.3
F	19.3	58.4
G	22.5	59.8
H	38.3	53.3
I	22.2	66.5